MDPI

Research on the Evolution of Snow Crystal Necks and the Effect on Hardness during Snowpack Metamorphism

Jie Wei, Peng Lu *, Shengbo Hu, Qiuming Zhao, Shunqi Yuan, Puzhen Huo and Qingkai Wang

State Key Laboratory of Coastal and Offshore Engineering, Dalian University of Technology, Dalian 116024, China; jiewei@mail.dlut.edu.cn (J.W.); hushengboandy@163.com (S.H.); qiumingzhao@mail.dlut.edu.cn (Q.Z.); yuansq_rex101@mail.dlut.edu.cn (S.Y.); hpz_ice@mail.dlut.edu.cn (P.H.); wangqingkai@dlut.edu.cn (Q.W.)
* Correspondence: lupeng@dlut.edu.cn

Abstract: To study the snow microstructure at various metamorphism times and extract the snow neck area, a constant density (200 kg/m^3) snow metamorphism experiment was conducted. The findings show that the neck region is mostly influenced by temperature, sun radiation, snow density and specific humidity, with wind speed having little effect. Additionally, we developed a multiple linear regression equation for the neck area under atmospheric forcing: "$S = 288T + 2E + 189\rho + 12{,}194V - 20{,}443RH - 42{,}729$". This equation accounts for solar radiation (E), temperature (T), snow density (ρ), specific humidity (RH) and wind speed (V). Notably, the above five factors can account for 84% of the factors affecting the neck area, making it a crucial factor. The relationship between snow hardness and neck area is correlated at 71%, and in later stages of metamorphism, the correlation may increase to 91%. Based on the neck area, the following hardness value prediction is made: "$H = 0.002764S + 67.922837$". This study documents the growth variations in the neck region of the metamorphic snow cover and elucidates the process by which outside factors impact the microstructure and macroscopic physical characteristics of the snow cover.

Keywords: snow crystals; microstructure; neck growth; metamorphism; hardness

1. Introduction

Snow is a significant part of the cryosphere and serves as a proxy for climate change [1]. As a result of global warming's effects on the cryosphere, snow's physical characteristics have changed. The thermodynamic properties and mechanical strength of snow are mostly determined by the interior crystal structure of the snow [2]. Complex ice skeletons are formed by the different shapes and binding interactions of snow crystals, and understanding the microstructure of snow can help with the advancement of snow engineering [3]. The thermal characteristics and mechanical indices of snow are crucial parameters to be considered in cold-region science and engineering. The process of how snow evolves will undoubtedly be significantly impacted by changing climate conditions as global warming progresses [4,5], requiring a careful examination of snow mechanics and snow hazard issues [6–10]. In the future, a crucial strategy for dealing with snow science and snow risks will be to link the microstructure and apparent physical properties of snow.

A morphological viewpoint has been used by earlier researchers to study the physical features of snowpacks, given the significance of these qualities and the impact of metamorphism on them. The primary factor impacting the macroscopic physical properties of snow during snow metamorphism is the modification of the microstructure of snow crystals, notably the necks. A neck is one of the many microstructural characteristics of snow. The narrow area between two ice crystal grains is referred to as the neck, and it starts where the surface curvature changes from being outwardly convex to inwardly concave [11]. Therefore, the neck area is the region in the connecting point of the two necks

of two adjacent ice crystals. Hardness is one of the mechanical factors of snow accumulation, and the neck, being the weakest region of the snow crystal, greatly influences its mechanical properties. According to the earlier definition of hardness as the resistance to plastic deformation, subsequent research by Mellor [12] and Lee [13] suggested that the hardness of the snowpack can be thought of as a particular type of compression in the presence of side limits, with a strong correlation between the hardness value's magnitude and the snowpack's density and the state of its lateral confinement. Lateral confinement refers to the limitation of lateral displacement of snow by using restraint components in experiments. Its deformation characteristics are determined by the stresses that are transferred between the grains and the movement of the grains under natural conditions. The snow's continuous densification over time causes the snow hardness value to continuously increase over a certain period of time, with a tendency to increase with the snow depth [14]. Like other physical characteristics, snow hardness is largely influenced by the metamorphism between snow crystals. The bonding or necking between adjacent grains during the metamorphic process results in ice deposition at the contact points, and with densification and particle coarsening [15], the snow crystal necks become larger, and the snow becomes denser. Scholars have researched the microstructure of snowpacks, particularly the necks of snow crystals. Libbrecht et al. [16] conducted experimental studies on the growth rate of ice crystals on different surfaces, determined the morphology of snow crystals at different temperatures and supersaturation, and obtained the growth patterns of snow crystal shapes and neck bonds. Gubler et al. [17] studied chain-shaped snow crystals and used ice chains to describe the load-bearing capacity of snow by calculating the length of grain bonds, thus improving the model for analyzing snow intensity using snow crystal shape and neck bond growth. Edens and Brown et al. [18] examined the reasons for alterations in the neck area caused by significant deformation as well as the impact of new bond creation on the neck area. Brown et al. [19] extended the neck growth model to porous metals and proposed an intrinsic law based on the deformation of grains and grain bonding to explain the changes in the microstructure of snow under pressure. Snow deformation behavior was explained by Kry [20] using the idea of chaining, and Hansen and Brown [21] created a statistical model utilizing bond radii to describe the structure of snow particles. Less research has been performed on the impact of snow microstructural changes on snow hardness during metamorphism; however, past studies have concentrated on the development of an ontological model for snow. An important background for ice and snow engineering problems is the connection between the microstructure of snow and its apparent mechanical hardness.

In contrast to previous studies, this study continuously observed snow samples in the field to determine how their microstructure and macroscopic physical properties, such as hardness, changed as the snow underwent natural metamorphosis. The results, which were obtained via the stereology method to analyze the impact of metamorphism on snow from the viewpoint of microstructure, contribute to a deeper comprehension of snow mechanics and provide a point of reference for describing changes in snow crystal morphology and overall strength [22].

2. Materials and Methods

2.1. Overview of the Research Area and Research Equipment

The experiment was carried out at the Songhua River Dadingzi Mountain Hydroelectric Hub Comprehensive Test Site in Harbin City, Heilongjiang Province, China, between 24 December 2022 and 12 February 2023. The site coordinates are 46°39′ N and 127°25′ E (location of the red star marker in Figure 1). For approximately 130 days of the year, the Harbin section of the Songhua River is frozen over [23], and many snowfall events and extended periods of cold weather have led to the growth of local snow and ice sports, including skiing, cold-water fishing, winter fishing, and winter rallies. The thermal and physico-mechanical characteristics of snow are of guiding significance for the economic development of the area as well as the prevention and control of natural disasters because

snow is a significant tourism resource in the region. A temperate monsoon environment with notable seasonal changes prevails in the research region. In the cold, dry winter, it is dominated by temperate continental air masses, and in the hot, humid summer, it is dominated by temperate oceanic air masses or modified tropical oceanic air masses. The average temperature over the course of the year is 4.3 °C, with the average temperature in January being approximately −18.3 °C and the average wind speed being approximately 2.8 m/s. The average temperature and wind speed in February are approximately −14 °C and 3.0 m/s, respectively. The snowfall season is centralized from November to January. During this period, the greatest snow depth is approximately 41 cm, with an average precipitation (snowfall) of 23.6 mm [24].
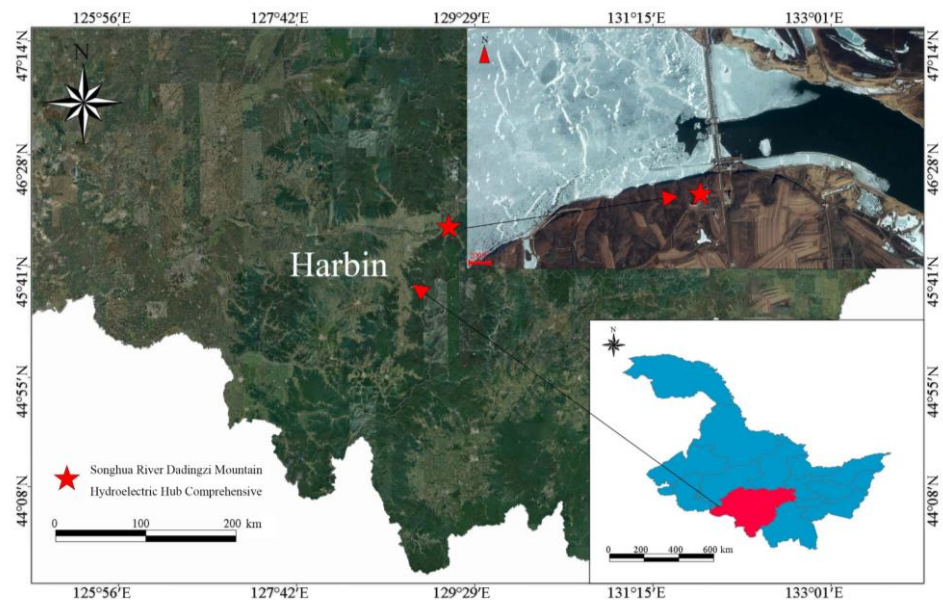

Figure 1. Location of the research area.

　　Snow temperature field observations were performed using temperature sensors for platinum resistance temperature sensors (accuracy of ±0.1 °C), while snow depth was measured using an ultrasonic ranging sensor (SR50A type (Campbell, Logan, UT, USA)) (accuracy of ±1 cm), both of which used a data acquisition instrument (Campbell CR3000 type(Campbell, Logan, UT, USA)) to collect data. The temperature chain layout is shown in Figure 2a. A JT-H6 industrial microscope(Jingtuo Youcheng Co., Ltd., Shenzhen, China) was used to observe the snow crystal microstructure, as illustrated in Figure 2b. The magnifying range of the microscope ranged from 0.7 to 4, and calibration was necessary to establish the scale before viewing. A dynamic resistive strain gauge (YD-28A type(East China Electronic Instrument Factory, Shanghai, China)) was used to connect an electronically controlled penetrometer [25] to the acquisition equipment (VK701H+(Weijingyi Electronics Co., Ltd, Shenzhen, China)), as illustrated in Figure 2c, to measure the hardness of the metamorphic snow. Figure 2d illustrates how the ring knife approach was used to sample the whole snowpack to determine the snowpack density.

2.2. Experimental Design

　　Drawing upon previous research and with the aim of facilitating a closer examination of the microstructure of snow crystals, snow was collected from the same snowfall, and its density was established at 200 kg/m^3. The prepared snow samples were compacted layer by layer in a detachable wooden test box, which had a cross-sectional area of 25 × 25 cm and a height of 60 cm. To ensure the maximum possible initial uniformity of internal density in the snow samples, each layer was 10 cm thick. The initial internal density of the snow specimens was preserved as uniformly as possible through layered compression.

Snow samples that received solar radiation were placed in an open, unobstructed area for natural metamorphism, whereas snow samples without solar radiation were placed on the shaded side of the building and covered with a shading canvas to ensure they were not influenced by solar radiation.
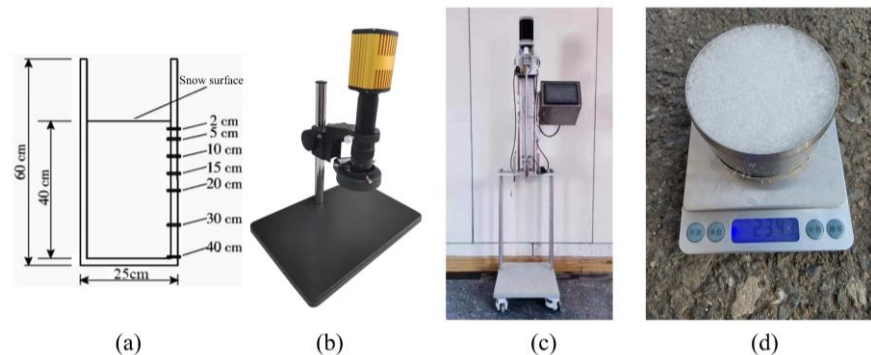

Figure 2. Parts of the test equipment. (**a**) Snow test chamber and sidewall temperature sensor arrangement (the uppermost snow surface as the origin); (**b**) industrial microscope; (**c**) electronically controlled penetrometer; (**d**) ring knife.

Temperature sensors were positioned in holes drilled in the wall of the test chamber exposed to solar radiation to monitor temperature changes in the vertical direction of the snow layers. Additionally, a temperature sensor was installed for continuous monitoring of the air temperature, while a sensor for determining the ambient temperature was placed in a radiation shield to prevent any temperature increase due to sunlight exposure. Snow temperature and air temperature were sampled once per minute. The upper boundary of the specimen was in direct contact with the atmosphere and solar radiation, whereas the lower boundary was separated by a wooden board and a thick layer of prepacked snow on top of the soil. A significant amount of snow was accumulated at the bottom and around the periphery of the test chamber to reduce the impact of temperature variations on the underlay and to ensure uniformity of the test results.

To observe the microstructure of the snow specimen, it was necessary to open the sidewall of the wooden box and use an ice scraper to gently remove the snow particles in layers to avoid destroying the original structure between the snow crystals. The extracted snow crystals were laid flat on a black acrylic plate after cooling and adjusting the magnification and focal length of the microscope to obtain the best image. The lower end of the electronically controlled penetrometer penetration rod was connected to a conical cone with a tip angle of 60° and a base diameter of 30 mm, and the penetration rate was set at 15 mm/s. The penetration point was the center of the specimen, which was penetrated vertically to the bottom of the test box to stop the test, and the test data collected by the tension transducer were recorded. At the beginning of the metamorphic effect, the snow crystals changed more rapidly. The test interval was two days, and four days later, the test interval was changed to five days to ensure that the number of snow samples was sufficient. The test process and test snow sample storage are shown in Figure 3.

For each test, photographs of the snow crystals were taken in accordance with the four-layer stratification that occurred during compaction. When processing the photographs, preference was given to clearer photographs. An industrial microscope magnification scale was used to measure the actual area, circumference, and equivalent diameter of the neck region in the photographs. To ensure the accuracy of neck region selection, overlapping and mixed snow crystals were avoided, and necks with high resolution and obvious features were chosen. The method of selecting the neck area relied on manual identification and extraction. First, the area where two ice crystals were connected was found, and the four inflection points where the edge profile of the ice crystal changed from convex to concave were identified, i.e., the four points where the curvature of the edge profile of snow crystals with positive and negative signs changed (e.g., the four yellow dots in Figure 4b).

Afterwards, the two inflection points between different ice crystals were connected by smooth curves along the outer contour of the ice crystals (e.g., two red curves in Figure 4b), and the two inflection points of the same ice crystal were connected by straight lines (e.g., two blue straight lines in Figure 4b). The closed area formed by the two curves and two straight lines was the neck area needed for this test, and finally, the area, perimeter, and equivalent diameter of the box selected were calculated using image processing software. During calibration, the pixels occupied by the scale bar were marked as the corresponding actual length, and then the actual length and area of the selected area could be determined. Although errors in manual recognition are unavoidable, the change in neck area caused by incorrectly identifying the inflection point was much smaller than the total neck area, and the technique of calculating the average value by counting many different neck areas was also effective in minimizing the error.
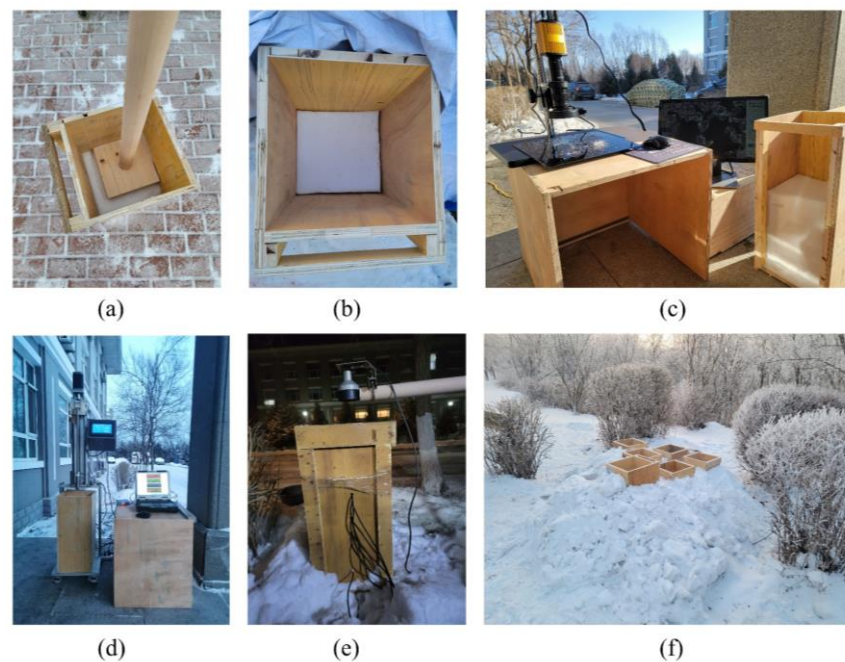

Figure 3. Observation of microstructure of metamorphic snow and penetration hardness test process and storage of snow samples. (**a**) New snow compaction; (**b**) compacted snow sample; (**c**) observation of the microstructure of snow crystals; (**d**) metamorphic snow penetration test; (**e**) measurement of temperature and snow depth of deteriorated snow samples from the solar radiation group; (**f**) storage of deteriorated snow samples from solar radiation groups.
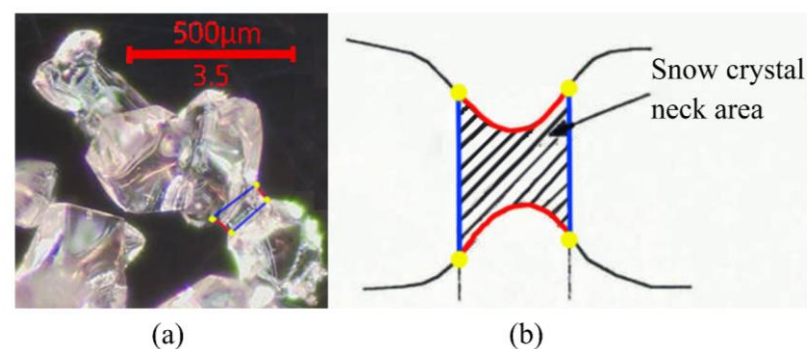

Figure 4. (**a**) Actual measurement of the neck area (magnification effect at 3.5 magnification). (**b**) Schematic diagram of the neck area.

3. Results and Discussion

3.1. Snow Metamorphosis

Figure 5 depicts the evolution of the air temperature, solar radiation group snow box profile temperature, snow density, hardness, and snow crystal neck area observed in the field over time.
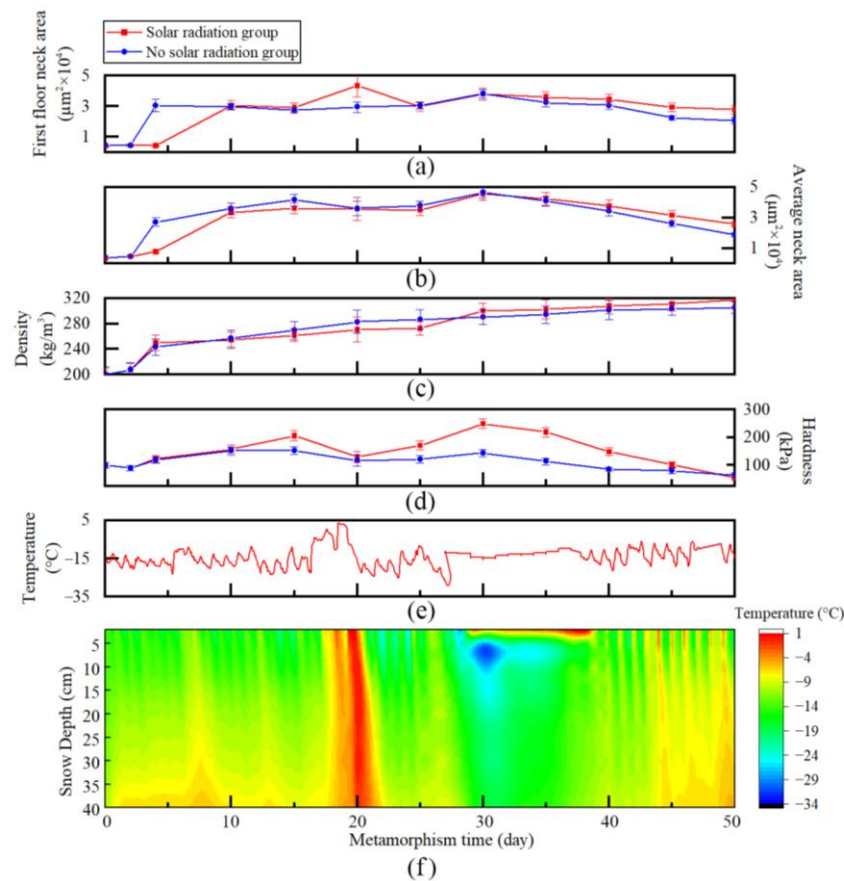

Figure 5. Changes in physical quantities over time during the experiment (**a**) neck area of the first layer of snow; (**b**) average neck area of snow; (**c**) density of snow; (**d**) hardness of snow; (**e**) temperature; (**f**) snow profile temperature of solar radiation group samples.

The test lasted for three months, from December to February of the following year, with average temperatures of -15.76, -14.48, and $-12.86\,°C$, respectively. On the eighteenth day of the test, the temperature increased significantly, moving to above zero. The average snow crystal neck area fell over the following three days, and the profile temperatures inside the snow box climbed to various degrees, but the neck area of the top layer of snow grew. The diurnal temperature fluctuated significantly from the forty-first day to the forty-fifth day of metamorphosis, and the temperature of the snow in the snow box displayed alternating warm and cold oscillations.

The neck area of the snow crystals rose prior to thirty days of metamorphosis, and the hardness values also gradually increased, as can be observed by combining plots a, b, and d in Figure 5. The first layer's neck region was more susceptible to the effects of temperature, particularly when warming caused a decrease in the neck area of the lower snow crystals. The snow crystal neck area decreased, and the hardness value also decreased at the later stage of metamorphosis or after thirty days. As shown in Figure 5c, the snowpack density rose over time; however, its rate of change was concentrated in the metamorphic period, since the collapse rate in the latter phase slowed.

The error bar records the error situation during repeated experiments. For the penetration test of snow hardness determination, limited by the number of wooden boxes and the

long metamorphism time, three wooden boxes were used for hardness testing each time. A single wooden box underwent three to four different penetrations, and its hardness value was the average of the final results, with relatively small dispersion. When measuring the neck size of snow crystals, the selected snow crystals came from multiple locations on the sidewalls of the snow layer. For snow layers at the same depth, we selected three to five locations parallel to the profile to extract snow crystals. We sprinkled them separately on the acrylic board and selected clear positions to take photos, extracting about ten images at a time. After summarizing the snow crystal photos of the same layer, 40–60 neck areas were selected by framing. Except for a few days when the temperature surged, the error in the neck area remained within a small range.

3.2. Analysis of Changes in Snow Crystal Neck Area

3.2.1. Effects of Solar Radiation

Figure 5a,b show the differences between the first layer and mean neck area over time curves for the two control groups, and it is clear that only the first layer, or the neck area of the 10 cm snow depth on the upper surface, of the snow specimens stored in wooden boxes was strongly affected by solar radiation (Figure 5a), with a difference of 13,913 μm^2 on the twentieth day. With a difference of 434 μm^2 on the twentieth day, the difference between the sun radiation group and the control group for the mean value of the neck area of each layer was not significant (Figure 5b).

The capacity of solar radiation to penetrate the snow layer makes it a crucial physical factor in changing the temperature of snow. Even if 90% of the incident radiation is reflected by snow, solar radiation will modulate the snow temperature and alter the snow temperature gradient either directly or indirectly [26]. The most significant and direct factor determining the warming of the snow specimen is the warming brought on by the absorption of solar radiation in the snow layer, which is more effective than heat conduction within the snow layer. This is reflected in the obvious temperature change in the snow in the upper 20 cm of the snow layer, and the closer to the snow surface it is, the more drastic the change in temperature is [27]. The borders of the wooden box that were utilized in this experiment always had a masking effect on the incoming sun radiation due to its height of 60 cm and initial snow thickness of 40 cm. Only the neck area of the snow crystals in the top 10 cm of the surface layer fluctuated considerably throughout the experiment, in contrast to the natural snowpack, which has an open surface without boundaries and solar radiation can affect a snow depth of up to 20 cm.

3.2.2. Effects of Temperature

Only the snow specimen profile temperature samples that received sun radiation were monitored for temperature because there were only a restricted number of collection devices in this experiment. The process of metamorphosis continued until the eighteenth day, when temperatures climbed above zero (Figure 5e). As a result of the temperature increase, the temperature of all layers of the snow specimen increased, and sublimation and condensation intensified. While the area of the surface snow necks rose, the sizes of the second, third, and fourth snow necks all shrank significantly (Figure 5a). The influence of heat flow in the underlying land determines temperature changes at the lower boundary of the snowpack, whereas temperature changes at the upper boundary of the snowpack are primarily influenced by solar radiation received at the snow surface and heat absorption and excretion during heat exchange on the snow–atmosphere contact surface [28]. Due to high-temperature sublimation, all snow layers other than the surface layer have a greater vapor flux and a contraction of the neck area. When the first snow crystals come into contact with the rising vapor flux from the lower snow surface, they precipitate, increasing the neck area of the first snow surface. The decrease in neck area caused by sublimation, however, is generally significantly greater for the entire snow sample than the rise in neck area caused by precipitation from adsorbed ice crystals (Figure 5b).

The curves of the snow crystal neck area relative to the air temperature for the solar radiation group are shown below, which combine the average neck area and air temperature during metamorphism in Figure 5b,e. The fitted curves are presented in Figure 6. Since the power metamorphism at the start of the fresh snow metamorphism is significantly larger than the temperature metamorphism, the fine snow whose metamorphism was carried out for up to ten days and beyond was selected for the statistics. Figure 6 shows that although the temperature and the neck are are adversely associated, the relationship is not particularly significant.
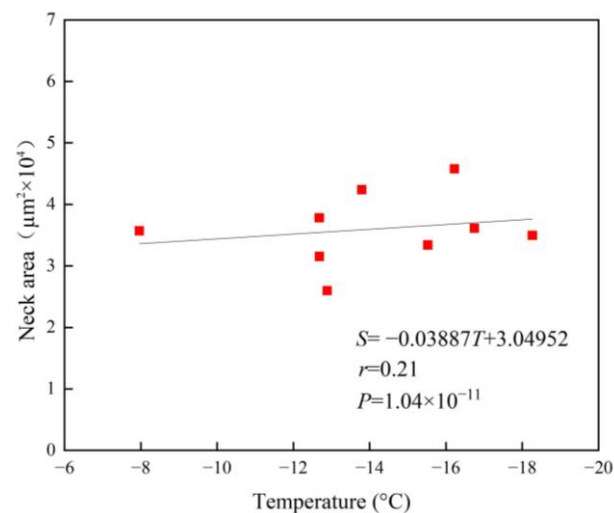

Figure 6. Relationship curve between temperature and neck area of the solar radiation group.

Due to the snow layer's strong insulation properties and low thermal conductivity, there is a temperature differential between the snow layer and the surrounding air. As a result, the snow crystal neck area's response to changes in air temperature lags slightly. Temperature is still one of the most significant factors influencing snow metamorphosis, despite the low correlation coefficient between the change in neck area and air temperature during snow metamorphosis. Lehning [29] considered grain growth and cross-layer mass transport as two distinct processes, with temperature serving as a crucial physical parameter that influences the transport of vapor fluxes within the snowpack, which has the potential to induce the transportation of water vapor, resulting in significant localized sublimation and precipitation within the snowpack. The growth of ice particles is a result of vapor diffusion among them, caused by the temperature gradient applied to the snow cover [30]. Furthermore, recrystallization leads to the formation of ice crystals, the strength of which is significantly influenced by temperature [31]. The impact of the snowpack's internal temperature on the neck region will be further examined in Section 3.2.4.

3.2.3. Effects of Snow Density

In the natural world, snow has a wide variety of densities, ranging from 300 to 550 kg/m^3. In this field environment, the recorded fresh snow density ranged from 70 to 150 kg/m^3 towards the conclusion of the snowstorm, and there were still significant voids after the snow was compacted with a density of 200 kg/m^3. As seen in Figure 5d, the rise in snow density in the region receiving solar radiation accounted for 45.2% of the overall density increase in the first ten days following the start of metamorphism, whereas the necking area quickly rose to 72.9% of the maximum necking area. In addition, the neck area of the snow in the region without sun radiation expanded to 77.7% of its maximum neck area, accounting for 51.9% of the overall density increase.

Following the statistics, Figure 7 displays the resulting curve of variation in the neck area and density of metamorphosed snow. In the thirty days between the start of the metamorphosis of the new snow and the start of the metamorphosis, the correlation

coefficients of density and neck area were 0.90 for the solar radiation group and 0.96 for the no solar radiation group. The correlation coefficients for density and neck area fell after thirty days of metamorphosis, and throughout the duration of the test, they were 0.77 for the group that received solar radiation and 0.69 for the group that did not. The necks can already exist as separate crystal structures in the later phases of metamorphism because of their long-term growth, and the newly formed crystals interact with the original crystals to generate new necks. Thus, the overall neck area appears to decrease as the number of old necks decreases and the number of new necks increases; however, the density of the snow always rises once the snow collapses, resulting in the opposite pattern of change in the neck area and density in the late stage of snow metamorphism and a nonmonotonic trend throughout the process.
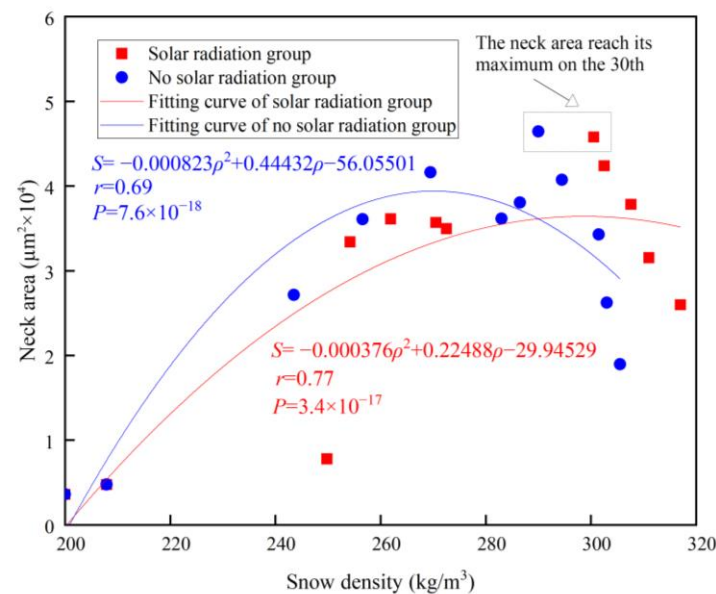

Figure 7. Relationship curve between snow density and the average neck area of each layer of snow crystals.

During the entire metamorphosis process, the experimental control groups exhibited the maximum neck area on the thirtieth day. Due to the exposure to light, the solar radiation group underwent a more intense metamorphosis, resulting in a more rapid elevation in density compared to that without solar radiation, with the peak in the neck area occurring at a later time. During the later stage of metamorphosis, the snow crystal morphology underwent a transformation from coarse snow to deep frost, with a notable decrease in the rate of density change compared to the initial stage.

3.2.4. Effects of Snow Depth

Based on stratifying the four layers of snow samples on the solar radiation surface and without the solar radiation surface (Figure 8), the area of the snow neck in each layer increases sequentially from top to bottom when there is no temperature fluctuation or when there is only a small amount of temperature fluctuation. The phenomenon described above in the relationship between temperature and snow neck area occurs when the temperature rises quickly for a brief period, causing the increase in the first layer's neck area to display a different pattern from the other three layers. The growth of the neck is a result of a fusion of pressure sintering, vapor diffusion, volume diffusion, and grain boundary diffusion. Over the course of seventeen to twenty-one days, the snow profile undergoes drastic temperature changes (Figure 5f), during which vapor diffusion takes over, leading to the generation of vapor from the lower snow crystals beyond the surface layer, which later condenses out of the surface snow crystals. If the external temperature does not experience significant

changes, pressure sintering will be the dominant mechanism, where the underlying snow crystals will carry the load from the self-weight of the upper snow layers. As a result, the bottom snow crystal neck experiences increased compression, normal force, and shear force transfer, which causes the grain structure to form early and with a larger area of the neck to accommodate the above additional strain.
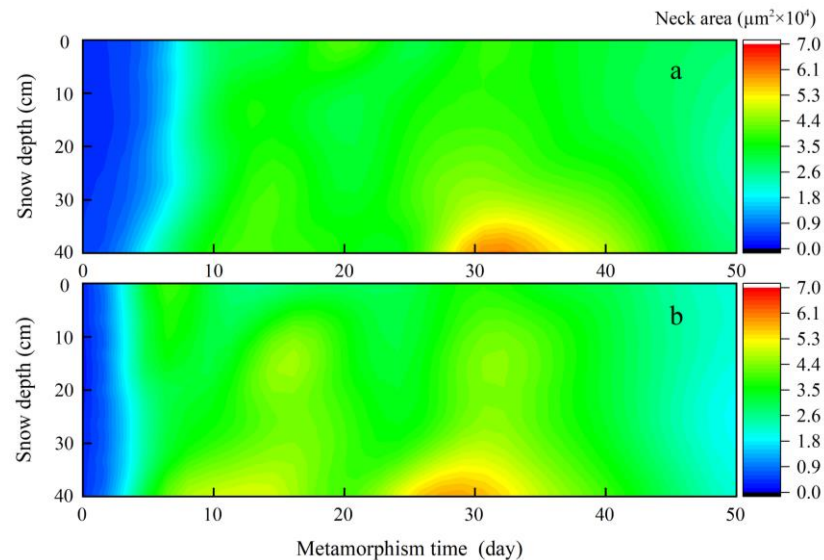

Figure 8. Changes in the neck area of snow crystals at different depths over time. (**a**) Changes in the neck area of snow crystals at different depths under solar radiation; (**b**) changes in neck area of snow crystals at different depths without solar radiation over time.

Figure 9a was created by plotting the temperature of the snow layer against the neck area of the snow crystals as they were measured in stages. The vertical snow pressure on the snow crystals in each layer was derived from the density and was used to determine the snow thickness using the snow layer settlement data collected by the ultrasonic range sensor. The four points from left to right in Figure 9b represent the average of the four layers of snow crystals in the snow box from the surface to the bottom at all metamorphic times. The points in Figure 9a cover the temperature and neck area of each layer during metamorphism, and since the snow layer temperature always varies with air temperature during metamorphism, the points are more discrete along the transverse axis and cannot be fitted after averaging the layers. The change in vertical load due to metamorphism is much smaller than the difference between snow layers, and so it can be calculated by averaging each snow layer. On the other hand, Figure 9b divides the changes in vertical load and neck area during metamorphosis of the four-layer snow specimens into four points after averaging and plots the error lines due to the changes in neck area and vertical load due to metamorphosis. The correlation in Figure 9a is better than the correlation of temperature in the neck area in Figure 6, and the snow profile temperature better reflects the effect on the neck area after accounting for the thermal conductivity of snow. However, the temperature is still less effective in describing the neck area, mainly because the effect of temperature on the neck of snow crystals is not an instantaneous process, and the description by the average value of the temperature does not fully reflect the metamorphic effect caused by vapor diffusion. Overall, the snow crystal neck area increases with snow depth, and the increase in vertical pressure contributes to the rise in the snow crystal neck area.

3.3. Relationship between Snow Crystal Neck Area and Total Crystal Area

Snow crystals undergo changes from needle-like, broad slab, and columnar morphologies to deep frost during metamorphosis, and the size of the snow crystals themselves constantly changes [32]. In order to explore the effect of snow crystal neck area on snow crystal size, Figure 10a statistically shows the change in the average size area of snow

crystals (S_t) with metamorphosis time (D). It can be seen that, excluding the days at the beginning of metamorphosis and the days when the temperature increased from the 18th day, the snow crystal area showed an increasing trend. The surface area of snow crystals was initially larger because new snow retained the intact dendritic structure. With the onset of metamorphism, the dendritic structure was compressed and gradually disappeared, and the snow crystal area contracted. During the days of rapid temperature rise, as analyzed in Section 3.2.2, the vapor diffusion of the snow crystals increased and the area contracted. However, for the entire metamorphic period, the individual fine-grained snow crystals gradually coalesced to display an increasing trend in overall snow crystal area.
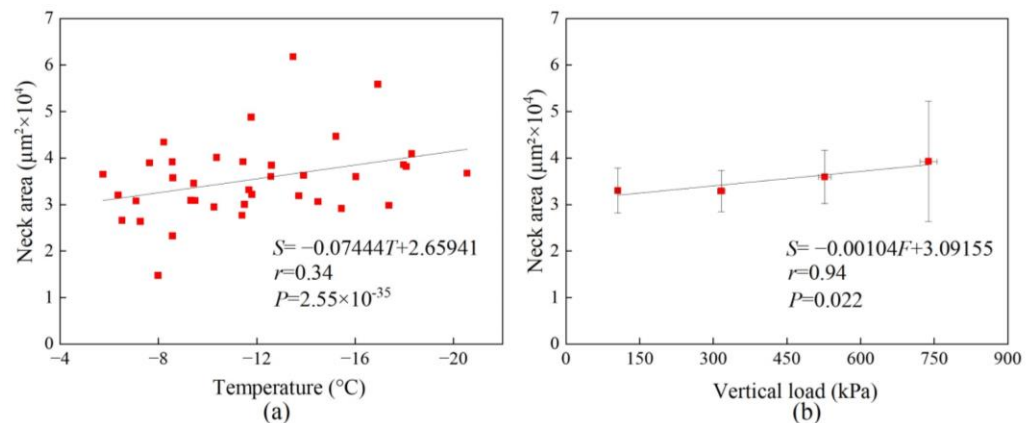

Figure 9. Relationship curve between neck area and solar radiation group snow (**a**) temperature and (**b**) vertical load.

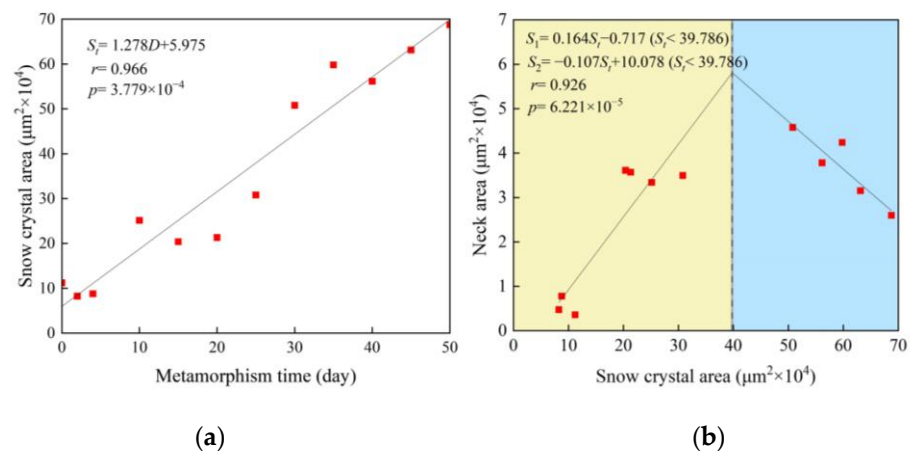**Figure 10.** Solar radiation group's (**a**) curve of mean snow crystal area with time and (**b**) curve of mean snow crystal area versus neck area (yellow and blue backgrounds represent different trends in the neck area and the snow crystal area).

As shown in Figure 10b, the neck area of snow crystals undergoes two stages with the variation of snow crystals. In the first stage (points covered by a yellow background in Figure 10, where the neck area of snow crystals can be described as the rising segment of S_1), the neck area increases with the increase in snow crystal area, and material exchange occurs between the two snow crystals through the neck. As the snow crystals increase in size, the neck, which serves as a material exchange channel, also gradually increases in area. In the second stage (points covered by a blue background in Figure 10, where the neck area of the snow crystal can be described as the S_2 descending segment), the neck area shows a downward trend as the snow crystal area increases. When the snow neck develops to a certain extent, its connection with the snow crystal changes, no longer presenting the shape described in Figure 4, but instead becoming an irregular shape close to the snow crystal.

More and more snow necks undergo the above evolution, leading to a decrease in neck area, while snow crystals continue to grow. At this time, the two show a negative correlation.

3.4. Relationship between Snow Crystal Neck Area and Hardness

The snow crystal neck region displayed an overall tendency to grow and then decrease as the number of metamorphism days increased. The snowpack hardness value peaked at approximately one month into the metamorphic process, and then it steadily declined as the neck region shrank, resulting from the formation of new crystals and necks at a later stage (Figure 5a,b,d). The following Pearson correlation analysis was performed using the snow hardness of the snow that received solar radiation from day 0 to day 50 of the metamorphic time, as well as the equivalent snow crystal grain diameter, neck circumference, neck area, and snow specimen density data, to further investigate the relationship between snow crystal microstructure and snow hardness (Table 1). With a correlation coefficient of 0.711 and passing the significance test at the 0.05 level, the results demonstrate a positive link between snow hardness and the neck area of snow crystal particles. To perform additional regression analysis on the influence of hardness, this article chooses the neck area of the snow samples.

Table 1. Correlation analysis of the hardness of metamorphic snow with the density and microscopic parameters of snow crystals.

	Snow Hardness (kPa)	Equivalent Neck Diameter (μm)	Neck Circumference (μm)	Snowpack Density (kg/m^3)	Neck Area (μm^2)
Snow hardness (kPa)	/	0.443	0.459	0.041	0.650 *
Equivalent neck Diameter (μm)	0.443	/	0.997 **	0.804 **	0.919 **
Neck circumference (μm)	0.459	0.997 **	/	0.783 **	0.926 **
Snowpack density (kg/m^3)	0.041	0.804 **	0.783 *	/	0.688 **
Neck area (μm^2)	0.650 *	0.919 **	0.926 **	0.688 **	/

Notes: * $p < 0.05$.; ** $p < 0.01$.

Based on a multiple linear regression analysis of the observed data, the correlation coefficient R between metamorphic snow hardness and the neck area of snow crystals was 0.711 (Figure 10), indicating a strong linear relationship between the two variables and positive overall regression effects. The regression equation's *p* value within 0.01, which was statistically significant and passed the significance test, showed that the neck area of the snow crystals in the snow specimens had a substantial impact on the snow hardness. Consequently, the regression equation for snow hardness in this examination scenario is presented below:

$$H = 0.002764S + 67.922837 \tag{1}$$

where *H* represents the predicted value of the snow hardness regression equation in kPa and *S* represents the snow crystal neck area in μm^2.

The snow crystal neck area and snow hardness have a good correlation, as shown in Figure 11. This finding demonstrates how many of the physical and mechanical characteristics of snow, including hardness and shear strength, are significantly influenced by the area around the snow crystal neck. The explanation for this is that ice particles may transfer loads to snow necks without experiencing significant deformation because they have a higher mass and are more rigid structurally than snow necks. The stresses within the snow crystals are exposed to the loading peak at the neck, similar to any cohesive granular material; in other words, the neck region bears the most stress during penetration tests. On the other hand, snow necks are more likely than ice grains to deform when

they are put under additional strain and start to give and flow. However, snow triaxial measurements reveal that the stresses at the snow neck are 5 to 50 times greater than those at the grains [33], which is sufficient to demonstrate the influence of the neck area on the physical characteristics of the entire snow body.
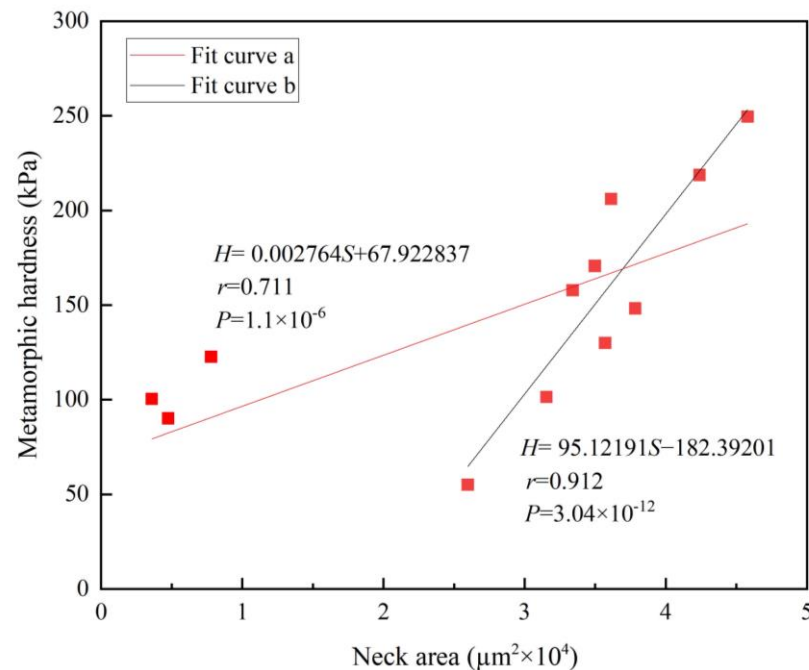

Figure 11. Curve of the relationship between the neck area and hardness of metamorphic snow in the solar radiation group (red line: fitting curve obtained based on all metamorphism times; black line: fitting curve obtained after ten days of metamorphism).

The three leftmost points in Figure 11 should be noted as they dramatically diverge from the general trend. These three measurements are the hardness and neck area taken on days 0, 2, and 5 at the start of the metamorphosis. The quick slumping and sintering modifications of the new snow intensify the heterogeneity of the metamorphosis of the layers and make the three measurements more distinct. If we account for only the metamorphism that occurs after ten days, as indicated by the black line, the correlation ($r = 0.912$) is noticeably larger when the same method is used to analyze the data. This result better illustrates how the neck of the snow crystals affects the snowpack's hardness.

4. Discussion

Combining field measurements and meteorological satellite data from the European Centre for Medium-Range Weather Forecasts, Table 2 lists the main meteorological conditions and the pertinent physical characteristics in the snow box of the solar radiation group during the test period. The mean ambient temperature readings, for instance, are based on the arithmetic mean of the temperature data collected in the field between the two tests. Two of the atmospheric forcing data for controlling snow cover metamorphism, solar radiation and wind speed, were sourced from the ERA5 Land dataset of the European Centre for Medium Range Weather Forecasts. The selected grids (46°36′ N–46°42′ N, 127°24′ E–127°30′ E) covered the experimental site (46°39′ N, 127°25′ E), with a time resolution of one hour and a spatial resolution of $0.1° \times 0.1°$. The data were collected by the Copernicus Climate Change Service (https://cds.climate.copernicus.eu/ (accessed on 1 April 2023)) and distributed at no cost through the Climate Data Store. The data from ERA5-Land have been applied to northeastern China on several occasions [34], and the data are in good agreement with the measured values [35]. Snow is a porous three-phase structure, and air humidity directly affects the surface of snow to change its moisture content and

affect its metamorphism [36,37]. Considering the lack of humidity data in ERA5 Land, data from the nearest Bayan County meteorological station (46°3′ N, 127°23′ E) were selected, and the data were collected from the National Meteorological Information Center China Meteorological Data Network (http://www.nmic.cn/ (accessed on 1 April 2023)).

Table 2. Changes in the neck area of deteriorated snow cover and its influencing factors over time.

Days to Metamorphism (day)	Average Neck Area (μm²)	Average Ambient Temperature (°C)	Cumulative Solar Radiation (W·h/m²)	Snow Density (kg/m³)	Average Wind Speed (m/s)	Average Specific Humidity (g/kg)
0	3593.9	−13.5	1137.4	200.0	2.9	0.9
2	4750.5	−16.3	1668.5	207.9	1.5	0.6
4	7791.9	−17.1	2086.2	249.8	1.8	0.7
10	33,403.8	−15.5	7002.8	254.2	2.8	0.6
15	36,121.9	−16.7	5639.1	261.9	1.9	0.6
20	35,700.4	−8.0	5586.1	270.5	3.3	1.5
25	34,969.3	−18.3	6280.4	272.5	2.3	0.5
30	45,791.3	−16.2	6335.2	300.5	2.3	0.5
35	42,391.0	−13.8	7763.6	302.5	1.8	0.3
40	37,831.3	−12.7	8366.3	307.6	1.8	0.7
45	31,541.3	−12.7	8270.2	311.0	1.7	0.8
50	25,977.3	−12.9	8117.7	317.0	2.1	1.2

After a significance test, the regression equation for the snowpack neck area had a correlation coefficient of $r = 0.919$. Below is the multiple linear regression equation for the test conditions' snowpack neck area:

$$S = 287.883T + 2.188E + 188.983\rho + 12,194.499V - 20,443.081RH - 42,729.115 \quad (2)$$

where S represents the snow crystal neck area in μm^2; T represents the average ambient temperature in °C; E represents the cumulative value of solar radiation in W·h/m²; ρ represents the snow density in kg/m³; V represents the average wind speed in m/s and RH represents the average specific humidity in g/kg.

Despite the high correlation coefficient of Equation (2), it is not directly evident how the five variables are correlated with the degree of influence on the neck area. Because of this rationale, the data analysis below involved a principal component analysis and factor analysis for the five variables that impact neck area in this statistic. The results of the principal component analysis that were obtained are presented in Table 3.

Table 3. Principal component results: total variance in explanation.

Ingredient	Initial Eigenvalue			Extraction of the Sum of Squares and Load		
	Total	Percentage of Variance (%)	Cumulative Percentage (%)	Total	Variance	Cumulative Percentage (%)
1	2.201	44.024	44.024	2.201	44.024	44.024
2	1.997	39.945	83.970	1.997	39.945	83.970
3	0.524	10.487	94.457	/	/	/
4	0.213	4.259	98.715	/	/	/
5	0.064	1.285	100.000	/	/	/

Table 3 shows that the first two principal components account for 84% of the variance, demonstrating that the neck region may be evaluated with some degree of certainty as the two extracted principal components can account for 84% of the five variables indicated

above. According to the aforementioned study, the two major components were identified as *Y*1 and *Y*2, and the linear combination of *Y*1 and *Y*2 was then obtained as follows:

$$Y1 = 0.613T + 0.286E + 0.273\rho - 0.404V + 0.551RH \tag{3}$$

$$Y2 = -0.057T + 0.611E + 0.629\rho - 0.382V - 0.284RH \tag{4}$$

The four atmospheric forcing factors mentioned above, along with snow density, responded to 83.97 percent of the variables that determine how much the snow crystals' necks vary, indicating that they may be the main factors influencing the neck area. Further factor analysis was carried out on Equations (3) and (4) to determine the normalized principal component score coefficients based on the coefficient analyses of the mean ambient temperature (*T*), cumulative solar radiation (*E*), snow density (ρ), wind speed (*V*) and specific humidity (*RH*), as shown in Figure 12. From Figure 12, it can be seen that the three factors with the highest proportion are density, solar radiation, and temperature. The specific humidity plays a supplementary role in explaining the changes in neck area, with wind speed contributing the lowest, at only 2.2%, and the neck area is not sensitive to its influence. Microstructure, temperature, and sedimentation all have intricate feedback relationships with one another [29]. Four different forms of atmospheric forcing changes affect the direction and rate of internal microstructural changes. The neck area represents microstructural changes that are intrinsic to changes in the internal physical properties of the snowpack. For instance, pressure sintering causes the growth of snow crystal necks and bonds [38], and the growth of the neck region boosts the thermal conductivity and heat transmission of snow while allowing the bonding strength between grains to grow and the settling rate to decrease. Since there is less of a temperature difference in the snow's vertical direction because of the enhanced heat transfer, there is less vapor flow, which prevents the growth of the snow neck. Additionally, when pressure sintering slows due to the decrease in settling, neck growth will also slow. Then, the aforementioned processes can be reversed or cycled in response to changes in the ambient temperature, with snow layer thermal anisotropy being a key factor in temperature gradient metamorphism [39]. The solar radiation directly heats the snow layer to affect the metamorphism of snow cover, and its contribution cannot be ignored. Humidity and wind speed also supplement the changes in the neck. Environmental humidity, as an important factor in the variation of moisture content in snow, plays a role in the growth of snow crystals. The wind speed directly affects the particle morphology and bonding mode on the top snow surface, leading to changes in transmittance and thermal conductivity, affecting the microstructure of surface snow and altering the energy input of the snow sample from the outside.
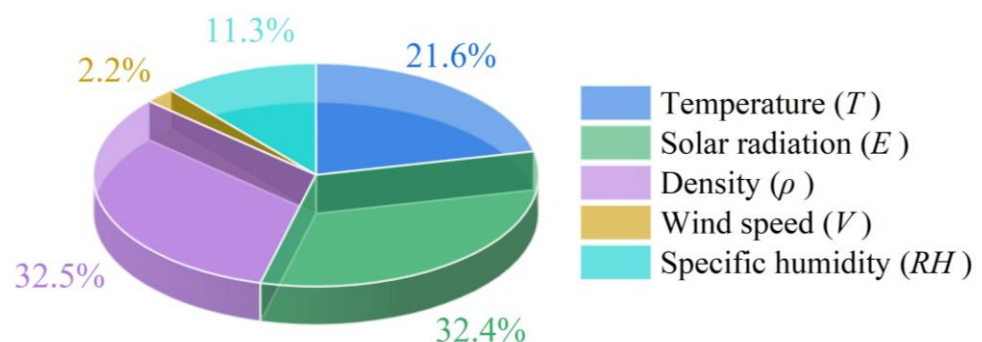

Figure 12. Normalized principal component score coefficient.

5. Conclusions

(1) The metamorphosis of the snow neck area is influenced by environmental factors including temperature, solar radiation, humidity and wind stress. The change in neck area is significantly affected by solar radiation and temperature, with the surface neck region absorbing water vapor from lower layers, resulting in an increase in area during

temperature surges. Conversely, the remaining snow necks undergo varying degrees of decrease due to vapor diffusion. The overall neck area displayed a declining pattern, which accounts for the fluffy appearance of the snow samples and the reduction in hardness numbers as the surrounding temperature rose. Humidity complemented the change in the neck area, while wind speed had the least effect.

(2) After ten days of metamorphosis, snow hardness had a strong positive association with the snow crystal neck area ($r = 0.912$). The weak link in the snow crystal linkage is the neck area, and one of the key determinants of the snow's mechanical properties is the area of the neck. The neck region better explains the anomaly that the metamorphosed snow's hardness initially rises and then falls, in contrast to the snow density, which constantly grows throughout the metamorphic process. Additionally, this demonstrates how modifications in the snowpack microstructure are inextricably linked to modifications in its macroscopic physical attributes.

(3) When atmospheric forcing is more steady, the neck area of each layer of the snowpack grows with snow depth. Pressure sintering, or the impact of the snowpack's makeup on the neck area, is the primary source of this phenomenon. The electronically controlled penetrometer hardness test further revealed that the hardness value increased as the depth of penetrated snow increased. After penetration, there was no discernible accumulation in the hole's vertical direction, indicating that the increase in hardness value was primarily brought on by an expansion of the snow neck's surface area in the depth direction as opposed to compression brought on by the vertical accumulation of snow during the penetration process.

In contrast to previous studies on snow microstructure, the present experiment was conducted to investigate the statistical changes in neck area during snow metamorphosis and the meteorological factors that affect it. Furthermore, the experiment aimed to elucidate how the snow neck area is affected by density, ambient temperature, wind speed, and solar radiation, as well as how the neck area affects snow hardness. In the future, further recording of more detailed environmental meteorological data and more microstructural parameters can be conducted. In addition, it is necessary to use improved methods to observe the snow accumulation during the melting period. At this stage, the nature of snow changes rapidly and is complex, which is of great significance for studying snow metamorphism.

Author Contributions: Conceptualization, P.L.; methodology, P.L. and J.W.; investigation, J.W., S.H., Q.Z. and Q.W.; data curation., S.H. and Q.Z.; formal analysis, J.W. and P.H.; visualization, J.W. and S.Y.; writing—original draft preparation, J.W.; writing—review and editing, J.W., P.L. and P.H.; project administration, P.L. All authors have read and agreed to the published version of the manuscript.

Data Availability Statement: Data are contained within the article.

Conflicts of Interest: The authors declare no conflict of interest.

References

1. Li, H.; Zhong, X.; Zheng, L.; Hao, X.; Wang, J.; Zhang, J. Classification of snow cover persistence across China. *Water* **2022**, *14*, 933. [CrossRef]
2. Calonne, N.; Flin, F.; Geindreau, C.; Lesaffre, B.; Rolland, D.R.S. Study of a temperature gradient metamorphism of snow from 3-D images: Time evolution of microstructures, physical properties and their associated anisotropy. *Cryosphere* **2014**, *8*, 2255–2274. [CrossRef]
3. Schneebeli, M. The importance of the microstructure of snow in nature and engineering. In Proceedings of the 1st International Conference on Design and Nature, Udine, Italy, 21 January 2002. [CrossRef]
4. Sarmiento, J.; Slater, R.; Barber, R.; Bopp, L.; Doney, S.; Hirst, A.; Kleypas, J.; Matear, R.; Mikolajewicz, U.; Monfray, P.; et al. Response of ocean ecosystems to climate warming. *Glob. Biogeochem. Cy.* **2004**, *18*, GB3003. [CrossRef]

5. Huo, P.; Lu, P.; Cheng, B.; Zhang, L.; Wang, Q.; Li, Z. Monitoring Ice Phenology in Lake Wetlands Based on Optical Satellite Data: A Case Study of Wuliangsu Lake. *Water* **2022**, *14*, 3307. [CrossRef]
6. Zhao, Q.; Li, Z.; Lu, P.; Wang, Q.; Wei, J.; Hu, S.; Yang, H. An Investigation of the Influence on Compacted Snow Hardness by Density, Temperature and Punch Head Velocity. *Water* **2023**, *15*, 2897. [CrossRef]
7. Xie, F.; Lu, P.; Li, Z.; Wang, Q.; Zhang, H.; Zhang, Y. A floating remote observation system (FROS) for full seasonal lake ice evolution studies. *Cold Reg. Sci. Technol.* **2022**, *199*, 103557. [CrossRef]
8. Han, H.; Yang, M.; Liu, X.; Li, Y.; Gao, G.; Wang, E. Study on the Constitutive Equation and Mechanical Properties of Natural Snow under Step Loading. *Water* **2022**, *15*, 3271. [CrossRef]
9. Ballesteros-Canovas, J.; Trappmann, D.; Madrigal-Gonzalez, J.; Eckert, N.; Stoffel, M. Climate warming enhances snow avalanche risk in the Western Himalayas. *Proc. Natl. Acad. Sci. USA* **2018**, *115*, 3410–3415. [CrossRef]
10. Medeu, A.; Blagovechshenskiy, V.; Gulyayeva, T.; Zhdanov, V.; Ranova, S. Interannual Variability of Snowiness and Avalanche Activity in the Ile Alatau ridge, northern Tien Shan. *Water* **2022**, *14*, 2936. [CrossRef]
11. Brown, R.; Edens, M. On the relationship between neck length and bond radius during compression of snow. *J. Glaciol.* **1991**, *37*, 203–208. [CrossRef]
12. Mellor, M. Engineering properties of snow. *J. Glaciol.* **1977**, *19*, 15–66. [CrossRef]
13. Lee, J.H.; Huang, D. Material point method modeling of porous semi-brittle materials. In Proceedings of the 9th World Congress on Computational Mechanics and 4th Asian Pacific Congress on Computational Mechanics, Sydney, Australia, 19–23 July 2010. [CrossRef]
14. Edens, M.; Brown, R. Measurement of microstructure of snow from surface sections. *Def. Sci. J.* **1995**, *45*, 107–116. [CrossRef]
15. Zhou, S.; Nakawo, M.; Hashimoto, S.; Sakai, A.; Narita, H.; Ishikawa, N. Densification and grain coarsening of melting snow. *J. Glaciol.* **2002**, *24*, 275–281. [CrossRef]
16. Libbrecht, K.G. Morphogenesis on ice: The physics of snow crystals. *Rep. Prog. Phys.* **2001**, *1*, 10–19. [CrossRef]
17. Gubler, H. Determination of the Mean Number of Bonds per snow grain And of the Dependence of the Tensile Strength of Snow on Stereological Parameters. *J. Glaciol.* **1978**, *20*, 329–341. [CrossRef]
18. Edens, M.Q.; Brown, R.L. Changes in microstructure of snow under large deformations. *J. Glaciol.* **1991**, *37*, 193–202. [CrossRef]
19. Brown, R.L. A volumetric constitutive law for snow based on a neck growth model. *J. Appl. Phys.* **1980**, *51*, 161–165. [CrossRef]
20. Kry, P.R. The relationship between the visco-elastic and structural properties of fine-grained snow. *J. Glaciol.* **1975**, *14*, 479–500. [CrossRef]
21. Hansen, A.C.; Brown, R.L. The granular structure of snow: An internal-state variable approach. *J. Glaciol.* **1986**, *32*, 434–438. [CrossRef]
22. Shapiro, L.H.; Johnson, J.B.; Sturm, M.; Blaisdell, G.L. Snow mechanics review of the state of knowledge and applications. In *US Army Cold Regions Research and Engineering Laboratory (CRREL) Report 97-3*; Cold Regions Research and Engineering Laboratory: Hanover, NH, USA, 1997. [CrossRef]
23. Yang, Q.; Song, K.; Hao, X.; Wen, Z.; Tan, Y.; Li, W. Investigation of spatial and temporal variability of river ice phenology and thickness across Songhua River Basin, northeast China. *Cryosphere* **2020**, *11*, 3581–3593. [CrossRef]
24. Wang, E.; Fu, X.; Han, H.; Liu, X.; Xiao, Y.; Leng, Y. Study on the mechanical properties of compacted snow under uniaxial compression and analysis of influencing factors. *Cold Reg. Sci. Technol.* **2021**, *182*, 103215. [CrossRef]
25. Feng, Z. Experimental Study on Snow Hardness and Its Testing Technology. Master's Thesis, Dalian University of Technology, Dalian, China, 2019. (In Chinese). [CrossRef]
26. Casado, M.; Landais, A.; Picard, G.; Arnaud, L.; Dreossi, G.; Stenni, B.; Prié, F. Water Isotopic Signature of Surface Snow Metamorphism in Antarctica. *Geophys. Res. Lett.* **2021**, *48*, e2021GL093382. [CrossRef]
27. Ma, H.; Liu, Z.; Sun, L.; Cai, G. A one-dimensional solution to the effect of solar radiation on the temperature field of snow cover: A case study of seasonal snow cover in the Western Tianshan Mountains of China. *Sci. Bull.* **1992**, *37*, 1205–1208. (In Chinese) [CrossRef]
28. Apaloo, J.; Brenning, A.; Bodin, X. Interactions between Seasonal Snow Cover, Ground Surface Temperature and Topography (Andes of Santiago, Chile, 33.5° S). *Permafrost Periglac.* **2013**, *23*, 277–291. [CrossRef]
29. Lehning, M.; Bartelt, P.; Brown, B.; Fierz, C.; Satyawali, P. A physical SNOWPACK model for the swiss avalanche warning-Part II. Snow microstructure. *Cold Reg. Sci. Technol.* **2002**, *35*, 147–167. [CrossRef]
30. Colbeck, S. Theory of metamorphism of dry snow. *J. Geophys. Res-Oceans* **1983**, *88*, 5475–5482. [CrossRef]
31. Pinzer, B.R.; Schneebeli, M. Snow metamorphism under alternating temperature gradients: Morphology and recrystallization in surface snow. *Geophys. Res. Lett.* **2009**, *36*, L23503. [CrossRef]
32. Donahue, C.; Skiles, S.M.; Hammonds, K. In situ effective snow grain size mapping using a compact hyperspectral imager. *J. Glaciol.* **2021**, *67*, 49–57. [CrossRef]
33. Bartelt, P.; von Moos, M. Triaxial tests to determine a microstructure-based snow viscosity law. In Proceedings of the International Symposium on the Verification of Cryospheric Models, Zurich, Switzerland, 14 January 2000. [CrossRef]
34. Yue, S.; Yan, Y.; Zhang, S.; Yang, J.; Wang, W. Spatiotemporal variations of soil freeze-thaw state in Northeast China based on the ERA5-LAND dataset. *Acta. Geogr. Sin.* **2021**, *76*, 2765–2779. [CrossRef]

35. Pelosi, A.; Chirico, G. Regional assessment of daily reference evapotranspiration: Can ground observations be replaced by blending ERA5-Land meteorological reanalysis and CM-SAF satellite-based radiation data? *Agric. Water Manag.* **2021**, *258*, 107169. [CrossRef]

36. Flin, F.; Brzoska, J.B.; Lesaffre, B.; Coléou, C.C.; Pieritz, R.A. Three-dimensional geometric measurements of snow microstructural evolution under isothermal conditions. *Ann. Glaciol.* **2004**, *38*, 39–44. [CrossRef]

37. Slaughter, A.E.; Adams, E.E.; Staron, P.J.; Shertzer, R.H.; Walters, D.J.; McCabe, D.; Catherine, D.; Henninger, I.; Leonard, T.; Cooperstein, M.; et al. Field investigation of near-surface metamorphism of snow. *J. Glaciol.* **2011**, *57*, 441–452. [CrossRef]

38. Hansen, A.C.; Brown, R.L. A new constitutive theoiy for snow based on a micromechanical approach. In Proceedings of the Davos Symposium, Davos, Switzerland, 29 January 1987.

39. Izumi, K.; Huzioka, T. Studies of metamorphism and thermal conductivity of snow. I. *Cold Reg. Sci. Technol.* **1975**, *33*, 91–102. [CrossRef]